Quaternary Science Advances 5 (2022) 100041

Contents lists available at ScienceDirect

Quaternary Science Advances

journal homepage: www.sciencedirect.com/journal/quaternary-science-advances

Vedde Ash constrains Younger Dryas glacier re-advance and rapid glacio-isostatic rebound on Svalbard

Wesley R. Farnsworth [a,b,*], Ólafur Ingólfsson [b,c], Erik S. Mannerfelt [d,e], Maarit H. Kalliokoski [a], Esther R. Guðmundsdóttir [a,f], Michael Retelle [b,g], Lis Allaart [f], Skafti Brynjólfsson [h], Mark F. A. Furze [b], Holt J. Hancock [b], Kurt H. Kjær [i], Anna J. Pieńkowski [b,j], Anders Schomacker [f]

[a] Nordic Volcanological Center, University of Iceland, Sturlugata 7, IS-102, Reykjavík, Iceland
[b] Department of Arctic Geology, The University Centre in Svalbard, NO-9171, Longyearbyen, Norway
[c] Institute of Earth Sciences, University of Iceland, Askja, Sturlugata 7, IS-102, Reykjavík, Iceland
[d] Laboratory of Hydraulics, Hydrology and Glaciology (VAW), ETH, Zurich, Switzerland
[e] Swiss Federal Institute for Forest, Snow and Landscape Research WSL, Switzerland
[f] Department of Geosciences, UiT The Arctic University of Norway, NO-9037, Tromsø, Norway
[g] Department of Geology, Bates College, Lewiston, 04240, Maine, USA
[h] The Icelandic Institute of Natural History, Borgum Norðurslóð, IS-600, Akureyri, Iceland
[i] GLOBE Institute, University of Copenhagen, DK-1350, Copenhagen, Denmark
[j] Institute of Geology, Adam Mickiewicz University, 61-606, Poznań, Poland

ARTICLE INFO

Keywords:
Cryptotephra
Glacio-isostatic adjustment
Restrained rebound
Relative sea level

ABSTRACT

The distal deposition of tephra from explosive volcanism has the potential to geochronologically constrain sedimentary archives and landforms. With this technique, we constrain a Late Glacial glacier re-advance on Svalbard and suggest that glacioisostatic emergence rates during the Younger Dryas chronozone were at least three times greater than previous estimates. The identification of cryptotephra (i.e., non-visible) horizons, outside the extent of visible fallout, has greatly expanded the field of application of tephrochronology. While the cryptotephra revolution has triggered a burst of investigations using low-concentration tephra to constrain distal sedimentary sequences, as of yet, few investigations have used this tool to constrain the age of glacial landforms. Here we constrain a moraine formed during a glacier re-advance (12.8–12.2 cal ka BP) into a high relative sea level during the early Younger Dryas chronozone, with the first identified occurrence of the Icelandic Vedde Ash on Svalbard. Low concentrations (~63 shards/g dried sediment) of the bimodal Vedde Ash (rhyolitic long axis *c.* 30–90 μm; basaltic *c.* 35–100 μm) were identified in a lake sediment sequence collected from the Heftyebreen glacier foreland, in a tributary valley to Grønfjorden, western Spitsbergen. Given that the cryptotephra was deposited within a lacustrine isolation basin, we further reconstruct a minimum rate of glacio-isostatic emergence during the end of the Late Glacial. Strong and longstanding evidence suggests Svalbard's west-coast cirque glaciers were less extensive during the Late Glacial than the Late Holocene. However, the Late Glacial Heftyebreen moraine suggests Svalbard glacier dynamics during this period may have been more complex.

1. Introduction

The distal deposition of tephra in far-field locations resulting from explosive volcanism is revolutionizing how we correlate and precisely date sedimentary archives and landforms (Lowe, 2011; Davies, 2015). Tephrochronology is unparalleled in spatial and temporal precision, providing the potential to investigate synchronicity or lag-response to climate forcing (Davies et al., 2012; Lane et al., 2013; Muschitiello et al., 2017). Cryptotephra studies - investigations of non-visible horizons of distally deposited ash - continue to further extend the spatial frontiers of this geochronological tool (e.g. Haflidason et al., 2019; Kalliokoski et al., 2020).

Visible tephra beds are most often used to constrain stratigraphic sequences (Lowe, 2011), but have also been correlated to glacial landforms (e.g., Schomacker et al., 2003; Benediktsson et al., 2015) as well as relative sea level (Rundgren et al., 1997; Brader et al., 2017). While

* Corresponding author. Nordic Volcanological Center, University of Iceland, Sturlugata 7, IS-102, Reykjavík, Iceland.
E-mail address: WesleyF@hi.is (W.R. Farnsworth).

https://doi.org/10.1016/j.qsa.2021.100041
Received 16 June 2021; Received in revised form 18 September 2021; Accepted 4 October 2021
Available online 9 October 2021

cryptotephra investigations have most commonly been used to constrain marine and lacustrine stratigraphic sequences (Zamelczyk et al., 2012; Wastegård et al., 2018; van der Bilt and Lane, 2019), as of yet, little focus has been placed on dating landforms or linking non-visible tephra to relative sea level. Cryptotephra has global potential in aiding regions with poorly constrained glacial and sea level histories, particularly in regions like the Arctic, where other forms of geochronology can be problematic (i.e. lack of organic material for ^{14}C dating, coal or carbonate rocks affecting radiocarbon ages; Wolfe et al., 2004; Timms et al., 2017).

A current synthesis of the Holocene glacial history of Svalbard highlights some of the geochronological challenges with dating glacial landforms and sea level changes especially during the last deglaciation (Farnsworth et al., 2020a). However, recent investigations have identified Middle and Late Holocene cryptotephra deposits in Svalbard and hinted at the chronological potential of these non-visible deposits (Kekonen et al., 2005; Wastegård and Davies, 2009; D'Andrea et al., 2012; van der Bilt et al., 2017). Identifying Late Glacial-Early Holocene tephras, such as the well dated Vedde Ash/Skógar tephra (VA; 12121±57 cal ka BP; (Mangerud et al., 1984; Norðdahl and Hafliðason, 1992; Andersen et al., 2006 Lane et al., 2012), would help constrain Svalbard's poorly dated glacier fluctuations (Farnsworth et al., 2018; Rasmussen and Thomsen, 2020).

We investigate lake sediments collected from an isolation basin

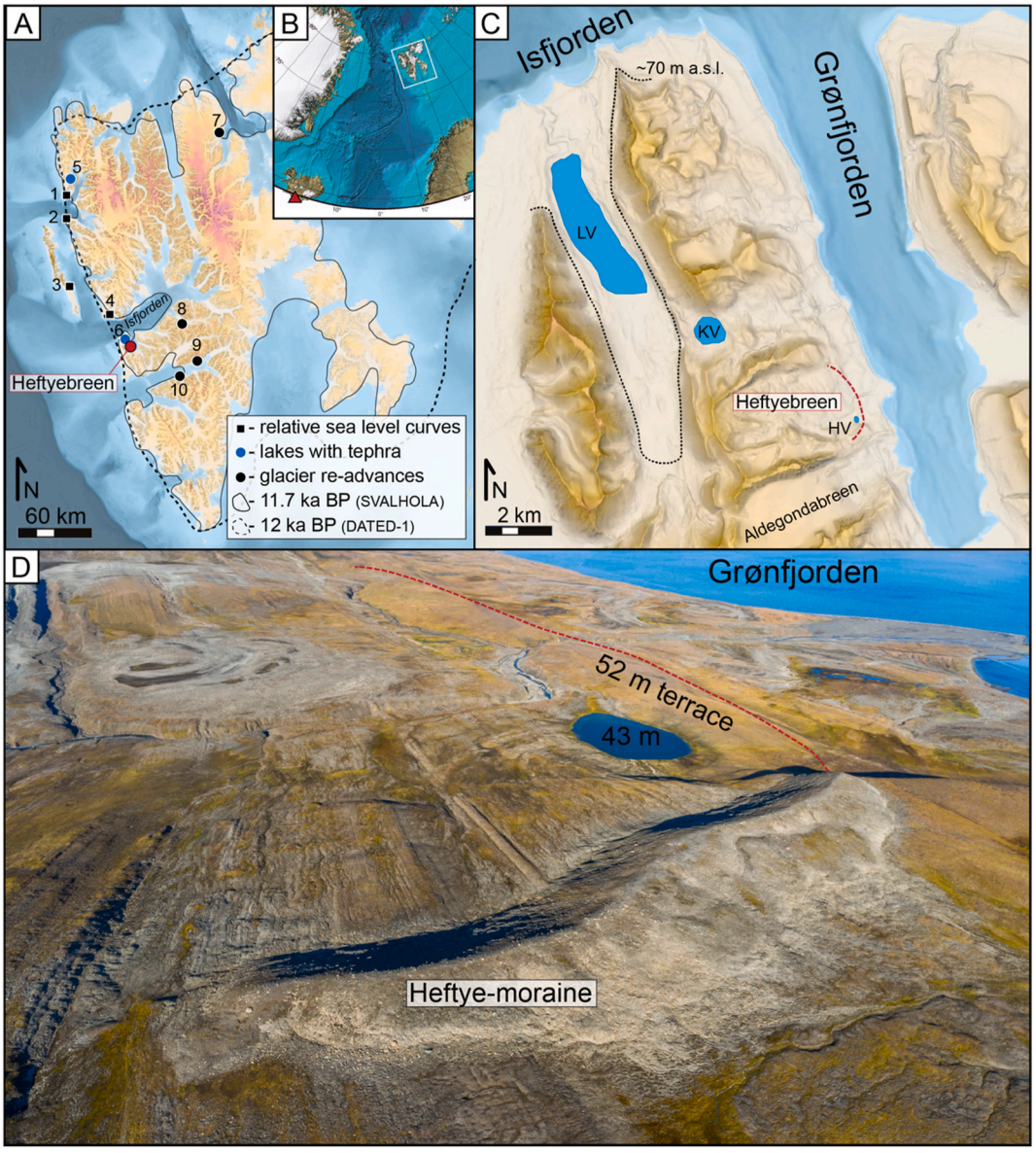

Fig. 1. Overview of the study site. A) Map of the Svalbard region. The Heftyebreen study area is marked with a red circle. Boxes indicate study locations of postglacial relative sea level curves (1-Mitrahalvøya, 2-Brøggerhalvøya, 3-Poolepynten, 4-Daudmannsodden). Blue circles mark lake sediment studies with previously identified cryptotephra (5-Hajeren, 6-Kongressvatnet) while black circles mark other Late Glacial – Early Holocene glacier re-advances (7-De Geerbukta, 8-Bolterdalen, 9-Gustavsdalen, 10-Bromelldalen). Ice margin time-slices outlined for 12.0 and 11.7 ka BP (Hughes et al., 2016; Farnsworth et al., 2020a). B) Inset map of the North Atlantic with Svalbard indicated. Red triangle marks the Katla volcanic system in southern Iceland. C) Map of Grønfjorden, with Linnévatnet (LV), Kongressvatnet (KV) and Heftyevatnet (HV) labeled. Heftyebreen catchment indicated with arcuate ridge symbolized by dashed red line. Dotted black line denotes 70 m a.s.l. contour mapped as the marine limit by Mangerud and Svendsen (1990). All bathymetry obtained from IBCAO version 3.0 (Jakobsson et al., 2012). D) Drone image (view towards north) with overview of the Heftyebreen foreland adjacent to Grønfjorden. Key elevations are indicated. The red dashed line marks the suggested continuation of the Heftyebreen moraine deposited into a high relative sea level. (For interpretation of the references to colour in this figure legend, the reader is referred to the Web version of this article.)

located within an abandoned moraine ridge on the west coast of Svalbard. The moraine is partial located above the regional post-glacial marine limit of c. 70 m a.s.l. and extends below this elevation expressed in a terrace c. 52 m a.s.l. The objectives of this study are to: i) determine the age of the moraine and the timing of basin isolation, ii) determine the age and origin of a cryptotephra occurring within the lake sediments, iii) consider the glacier re-advance in the study area in the context of other Late Glacial-Early Holocene re-advances on Svalbard, and iv) examine possible rates of Late Glacial emergence in the study area.

Here we present a well constrained glacier re-advance (12.8–12.2 cal ka BP) from western Svalbard which occurred during the first half of the Younger Dryas period (YD; 12.9–11.7 ka BP). The age of the glacier's end moraine is constrained by maximum- and minimum-limiting radiocarbon ages, which are further supported by the occurrence of the Vedde Ash as a cryptotephra within the isolation basin located inside of the moraine (Heftyevatnet; Fig. 1) Furthermore, the well-defined age of the Vedde Ash provides a close minimum-limiting constraint for the timing of basin isolation and allows us to reconstruct rates of Late Glacial emergence that are at least three times greater than previous studies suggest (Forman, 1990; Forman et al., 2004). Despite the increasing amount of sedimentary sequences dated by cryptotephra (Høgaas et al., 2021), this investigation of distally deposited tephra is one of the first to constrain an ice marginal position and relative sea level. We demonstrate how greater geochronological precision resulting from the successful application of crypto-tephrochronology can result in valuable quantitative constraints for past glaciers and relative sea-levels.

1.1. Setting

Heftyevatnet (informal name; 77.998°N, 14.149°E) is located in western Svalbard with a threshold at 43 m a.s.l. (Fig. 1). Heftyevatnet has an area of 1.5 ha within a 0.16 km^2 catchment and a maximum central water depth of 6.5 m (measured from lake ice). The regional bedrock is composed of NNW-SSE striking Early–Middle Triassic shale, siltstone and sandstone from the Sassendalen Group (Dallmann, 2015). At present, the lake catchment is non-glaciated and extends up to *c.* 130 m a.s.l. to the south with no active inlet or outlet. The lake basin is 730 m west of Grønfjorden, a N–S trending tributary fjord of Isfjorden which deglaciated prior to 11.5 cal ka BP (Fig. 1; Mangerud et al., 1992; Farnsworth et al., 2020a). A postglacial marine limit of ~70 m a.s.l. is described from a valley 6 km west (Mangerud and Svendsen, 1990) and the mouth of Grønfjorden (12 km north; Fig. 1D). The highest raised marine deposits within inner Grønfjorden, however, are located at *c.* 52 m a.s.l. comprising the terrace immediately to the east of Heftyevatnet (Fig. 1). However, depending on the timing of deglaciation, the relative sea level in inner Grønfjorden likely exceeded 52 m a.s.l.

2. Methods

2.1. Lake sediment coring

A series of lake sediment cores were retrieved using a hand-held piston coring system (with 205 cm long core tubes and a 64 mm inner diameter) from a small boat platform (August 2017) and spring lake ice (May 2019). Two overlapping piston cores were taken during each campaign in addition to a surface gravity core capturing the lake sediment-water interface in the central basin at 6.5 m water depth (Fig. S1). The region was field mapped during an August 2016 reconnaissance as well as during the 2017 field campaign.

2.2. Digital elevation model acquisition and processing

The Norwegian Polar Institute performed an aerial image survey (July 2010) over the study area, and the resultant 5 × 5 m Digital Elevation Model (DEM) is available publicly online (https://geodata.npolar.no). The DEM was used to derive elevation of Heftyevatnet and the surrounding landforms, as well as for visualization purposes (Fig. 2).

A semi-oblique (~20° off nadir) drone survey was conducted over the Heftye-moraine ridge (August 18th' 2019) at an altitude of approximately 120 m above ground level, using a commercial DJI Mavic 2 Pro drone. The drone captured 20 megapixel images with a focal length of 10.26 mm (28 mm in "35 mm equivalent"). The survey was processed in Agisoft Metashape 1.7.0 using rolling shutter compensation, an alignment quality of "High" (full resolution) and a dense cloud quality of "Ultra High" (full resolution) with the proprietary depth map filtering setting of "Aggressive". The image alignment yielded a low Root Mean Square (RMS) tie point reprojection error of 0.41 pixels (Carrivick et al., 2016; James et al., 2017), and a dense cloud point density of 627 points per m^2. The model was georeferenced using Iterative Closest Point (ICP; Besl and McKay, 1992) registration using the "xdem" Python package (xdem contributors, 2021) to reference 2010 DEM, yielding a vertical median difference of 0.00 m and a normalized absolute median deviation (NMAD) of 0.42 m. The NMAD was subsequently used as the georeferencing error of the model. With an average model diameter of 492 m, the 0.42 m vertical error equates to approximately 0.10° of rotational error ($\tan^{-1}$ (error/(0.5 x diameter))). After registration, DEM gridding was conducted with 0.05 m resolution per pixel. Subsequently an orthomosaic was created over the DEM. Minute error associated with model acquisition and processing should not affect geomorphological interpretations.

The bedrock surface underlying the moraine is near-horizontal with minor projected convex curvature (Figs. 1, 2). An attempt at modeling the bed of the landform was thus deemed viable to obtain a rough volume estimate. By masking out the landform, the remaining part of the DEM was fitted with a 5^{th} degree 2D polynomial to predict its general shape. The NMAD between the estimated polynomial surface and the true surface was 1.41 m. Using the presumption that the underlying ground is as homogeneous underneath the landform as around it, the bed of the landform could be predicted within the associated error margin. The volume of the landform was calculated from the mean estimated thickness within the ridge outline, multiplied by its planimetric area. The volume error was calculated as the polynomial NMAD multiplied by the same area.

2.3. Sediment core processing

Sediment core splitting, logging and analyses were conducted in the sediment lab and ITRAX core facility at the University of Copenhagen (Centre for GeoGenetics). High-resolution data including X-ray fluorescence (XRF), magnetic susceptibility (MS) as well as optical and radiographic images were collected for all cores after splitting. XRF measurements were conducted every 1 mm at 30 kV and 30 mA with a 30 s exposure with the ITRAX scanner. The core scanner has an X-ray source with a Rh (rhodium) anode (Croudace et al., 2006). For interpretation of the ITRAX measurements, Ti was normalized against the incoherent (inc) and coherent (coh) Rh scatter (Ti/(inc+coh)) to remove instrumental effects (Kylander et al., 2011). Furthermore, the Ca/Fe ratio signals minerogenic input and has been used to indicate the marine to lacustrine transition within isolation basins (Larsen et al., 2017; Schomacker et al., 2019).

2.4. Radiocarbon dating

Marine bivalve shells (*Hiatella arctica*), mixed benthic foraminifera and terrestrial macrofossils were radiocarbon dated at the Ångström Laboratory at Uppsala University, Sweden and LARA at the University of Bern, Switzerland. All radiocarbon ages were calibrated with Calib 8.2.0 (Reimer et al., 2020). Age-depth models were developed for the core sequence and the lowermost piston core with the Bayesian statistics code BACON (v. 2.5.2; Blaauw and Christen, 2011) within R studio (v. 3.3.3; R Core Team, 2020). The IntCal20 calibration curve was used on

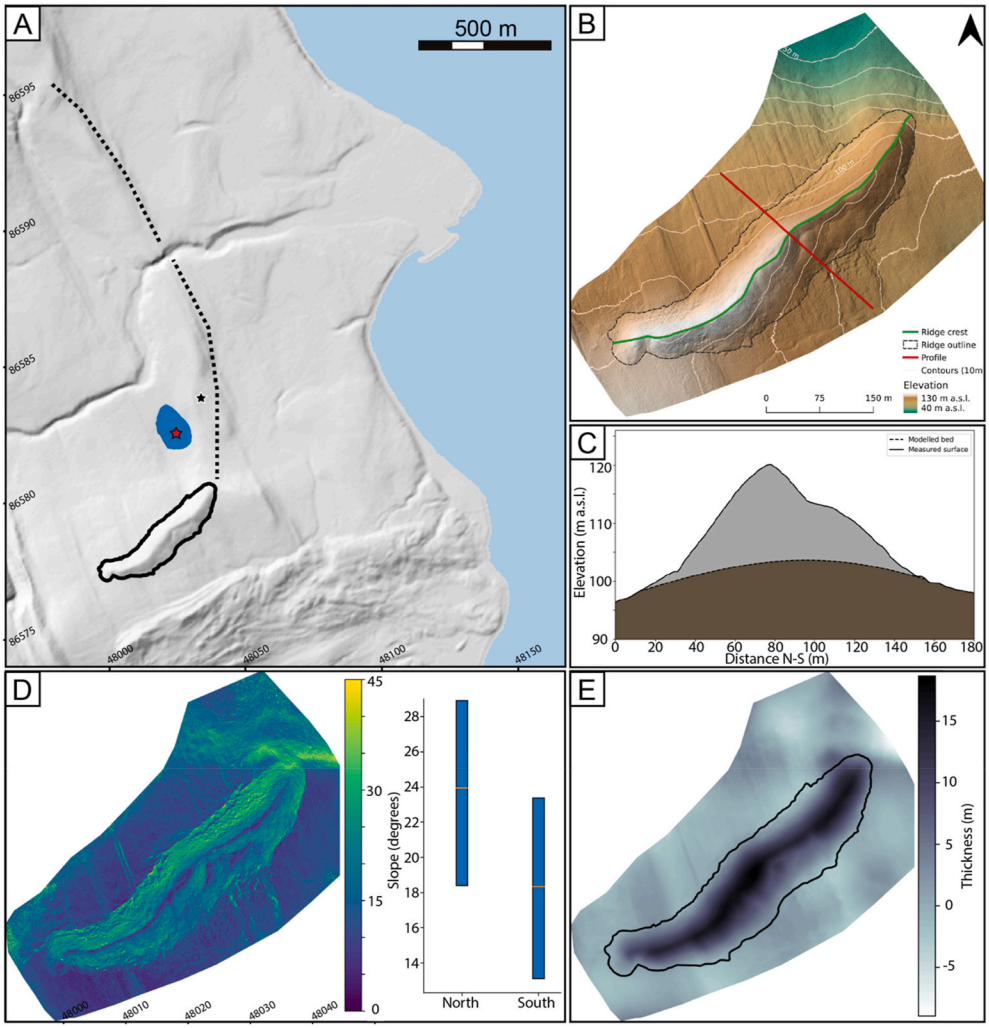

Fig. 2. Hill-shaded digital elevation model of the Heftyebreen foreland and high resolution map of the subaerial Heftyebreen moraine system. A) Norwegian Polar Institute DEM with outlined ridge and lake indicated. Stars mark core location (red) and approximate location of shell samples (black). B-E) Hill-shaded 0.1 m resolution drone DEM of sharp-crested ridge system with schematic cross-section model of landform thickness, slope inclination and ridge thickness projections. Ridge crest marked and cross profile indicated. (For interpretation of the references to colour in this figure legend, the reader is referred to the Web version of this article.)

terrestrial macrofossils while the Marine20 curve was used for shells and foraminifera (Heaton et al., 2020; Reimer et al., 2020). A regional delta R value of 70 ± 30 ^{14}C years was implemented during calibration (Mangerud et al., 2006). All ages are presented in calibrated kilo anno before present (cal. ka BP; BP = 1950; Table S1). Furthermore, radiocarbon ages from published relative sea level and glacier studies have been recalibrated and presented accordingly (Table S2).

2.5. Cryptotephra analysis

The lowermost sediments were surveyed for minute concentrations of non-visible tephra in accordance with developed practice (Pilcher and Hall, 1992; Timms et al. 2017; Kalliokoski et al., 2020). During the primary survey, the lower 60 cm of strata were sub-sampled at 3 cm resolution while the following 20 cm were investigated at 2 cm resolution. Roughly 1 cm^3 samples were dried (24 h at 105 °C), pestle-ground, ashed (4 h at 550 °C), bathed in 10% HCl, rinsed and then sieved in order to isolate the 10–90 μm fraction. Sediments were then subjected to heavy liquid density separation concentrating and dividing the potential volcanic glass into a silicic (2.3–2.5 g/cm^3) and a basaltic fraction (>2.5 g/cm^3; Turney, 1998). All survey samples were evaporated on glass microscope slides, mounted within Canada Balsam and capped with cover slides prior to inspection under a polarizing microscope. Tephra was identified based on distinct morphological characteristics including vesicularity, fluted structure and optical isotropy (Lowe, 2011). Where tephra was identified during the initial survey, the sediment core was again sub-sampled and surveyed once again at a 1 cm resolution in order to identify the stratigraphic interval with peak shard concentration. At this resolution tephra was counted, measured and described.

At peak intervals, cryptotephra samples were once again sampled for electron microprobe analysis (EMPA). The processing procedure was repeated although this time an acid digestion method was used in place of ashing (to avoid high temperature geochemical alteration; Dugmore et al., 1995). Volcanic glass was further concentrated on a microscope slide by individually picking shards with a micromanipulator equipped with a micro-syringe. Shards were embedded in epoxy prior to being sanded and polished to the surface (~15 μm). Before carbon coating, glass slides were inspected, mapped and shards were sketched in order to enhance EMPA-time efficiency. Major element composition was obtained by a standard wavelength dispersive technique on as many shards as possible for each sample (often in 2–3 rounds to avoid polishing away tephra). Cryptotephra was analyzed using a JEOL JXA-8230 SuperProbe with an accelerating voltage of 15 kV, beam current of 10 nA and a beam diameter of 5–10 μm (Kalliokoski et al., 2020). Standards (A99 for basaltic; and Lipari Obsidian for rhyolitic) were run in the beginning and end of each round of analysis (Table S3).

3. Results and interpretation

3.1. Heftyebreen moraine

A 540 m long sharp-crested, curvilinear ridge of poorly sorted

sediments is located to the southeast of Heftyebreen, in inner Grønfjorden. The SW-NE oriented ridge extends from ~80 to 160 m a.s.l. and overlies the NNW-SSE trending bedrock. Cross profiles from the drone DEM suggest a maximum thickness on the order of 16.5 m with a total landform volume of 0.40 ± 0.09 hm^3 (Fig. 2). The ridge has a slightly steeper NW flank with a slope inclination approaching ~30° (mean 24°; Fig. 2). The sharp-crested ridge is concordant with an adjacent terrace that has less relief and extends northward for ~1.5 km at an elevation of ~52 m a.s.l. (Figs. 1C and 2A; Fig. S2). Together, the moraine and the terrace delineate a nearly 2 km-long arcuate landform. This terrace is dissected by a channel draining catchment runoff into Grønfjorden. The terrace is composed of bedrock capped by a matrix-supported diamict with small boulders and shell fragments (Table S1). The flat-topped terrace morphology suggests deposition in a submarine environment. The mollusc fragments are interpreted as being ice-transported and redeposited, given their occurrence within a diamict, and likely originate from older marine deposits pre-dating the glacier re-advance. The terrace holds a small lake basin to the west, Heftyevatnet (Figs. 1C and 2).

We hypothesize that the sharp-crested curvilinear ridge and diamict capping the adjacent lower terrace were deposited contemporaneously as a moraine at the terminus of a glacier emanating from the Heftyebreen cirque. The sharp-crested ridge exhibits weathering and subaerial periglacial degradation characteristic of a sub-aerial depositional environment. The morphology of the corresponding lower elevation terrace as well as the shell occurrence suggests a subaquatic depositional environment (although it is unclear if the sediments were once subglacial). Thus, the palaeo-sea level when the moraine was deposited was above 52 m a.s.l. and below 80 m a.s.l. (lower extent of the sharp-crested ridge).

3.2. Heftyevatnet sediment sequence and tephra correlation

A ~300 cm long composite stratigraphy was developed for Heftyevatnet by correlating XRF data from one surface and two overlapping piston cores (sediment water interface = 0; Fig. S1). The lowermost meter of sediment (core HBP2b) was logged, scanned and analyzed in order to determine i) the age of the lowermost sediments in the basin (i.e. a minimum-limiting age for the Heftyebreen moraine) and ii) when Heftyevatnet isolated from the sea. The lower 100 cm is comprised of two lithostratigraphic units, recording the transition from a shallow marine environment during the Late Glacial (Unit 1) to a lacustrine setting during the Early Holocene (Unit 2; Fig. 3).

Unit 1 is a clayey-silty diamict extending from 240 cm to 300 cm depth in the composite stratigraphy. It is crudely horizontally bedded and matrix-supported. The diamict exhibits reduced X-ray transmission

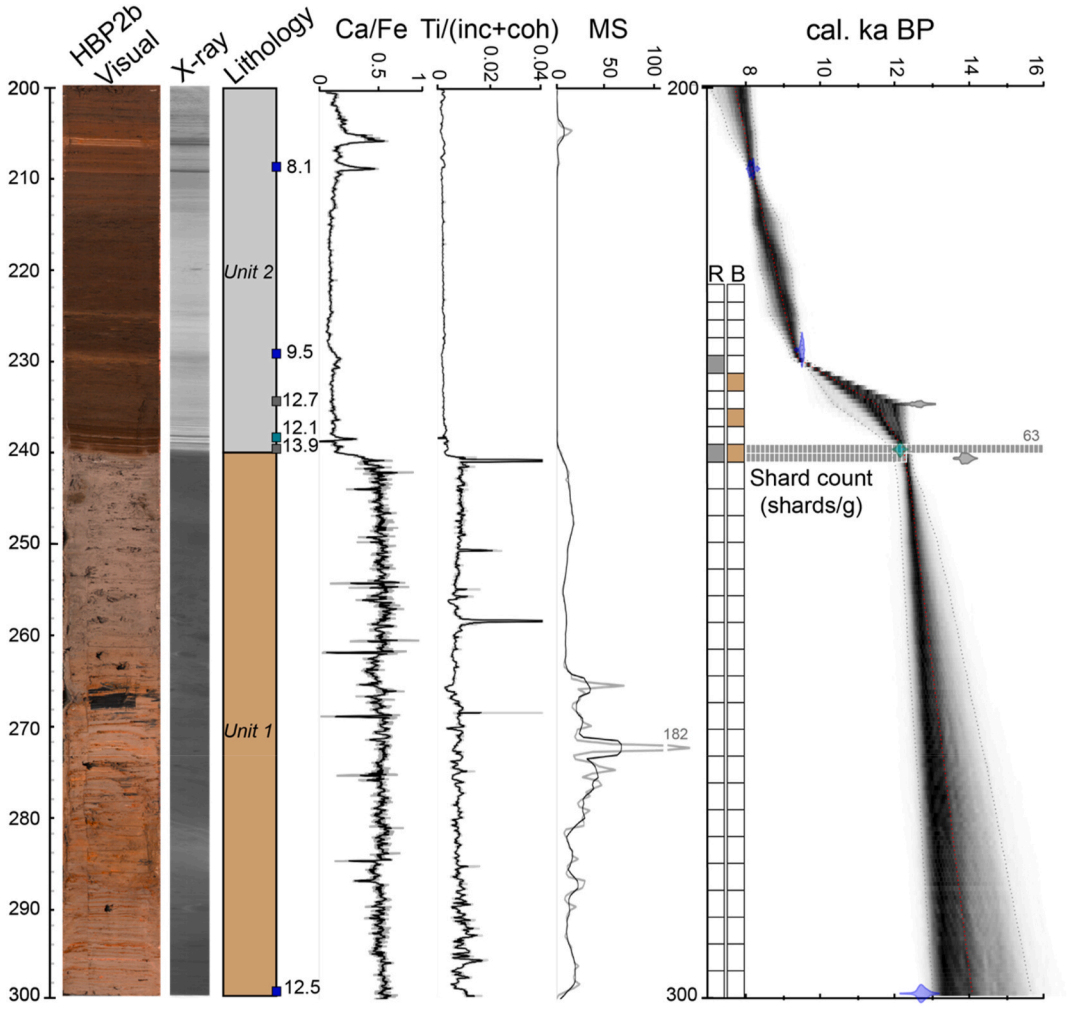

Fig. 3. Sediment proxies for the lowermost 100 cm of sediment core HBP2b, corresponding to 200–300 cm of the composite stratigraphy for the Heftyevatnet basin: core photograph, X-ray image, lithology with median calibrated ^{14}C (blue), anomalously old ^{14}C (grey) and tephra (green) ages. XRF data for Ca/Fe, Ti normalized by incoherent and coherent signal (Ti/inc+coh) and magnetic susceptibility (MS). XRF data plotted raw with 5 point running averages. Age-depth model developed from radiocarbon dates and VA cryptotephra. R and B symbolize shard concentrations of rhyolitic and basaltic tephra (respectively) per dried gram sediment. Details provided in Tables S1 and S3. (For interpretation of the references to colour in this figure legend, the reader is referred to the Web version of this article.)

as well as elevated Ca/Fe, Ti/(inc.+coh.) and magnetic susceptibility (Fig. 3). Furthermore, Unit 1 contains (presumed *in situ*) benthic foraminifera (predominantly *Elphidium excavatum* f. *clavata)*. No cryptotephra was identified in Unit 1 despite a 3 cm resolution survey of both silicic and basaltic weight fractions (Fig. 3). Unit 2 is a finely laminated brown gyttja extending from 200 cm to 240 cm depth in the composite stratigraphy. It contains intermittent beds of clayey-silt and exhibits moderate x-ray transmission with reduced Ca/Fe, Ti/(inc.+coh.) and magnetic susceptibility values characteristic of organic rich strata. While no foraminifera were identified in Unit 2, terrestrial and aquatic macrofossils are present throughout the strata (Fig. 3; Table S1). Cryptotephra was identified in the lower half of Unit 2 following a 2 cm survey of both silicic and basaltic weight fractions (Fig. 3).

Peak ash concentrations were identified within the lowermost interval of Unit 2, composed of finely laminated brown gyttja (sample HBP2_21A). Approximately 63 shards of rhyolitic and basaltic tephra per dried gram sediment were identified in the second cm of laminated organic rich lacustrine sediments overlaying the transition from marine basal sediments (Figs. 3, 4). Tephra shards were manually concentrated from the peak interval through micromanipulation prior to electron microprobe analysis detailing the major element composition of the glass (Fig. 4). Initial probe analysis suggested the silicic component was potassium-rich, characteristic of rhyolitic tephra from the Katla volcanic system, however not distinctive to the Vedde Ash (Lane et al., 2012; Haflidason et al., 2019). However, identifying and probing basaltic tephra in the same 1 cm sample interval, suggestive of a bimodal tephra horizon is unique to the Vedde Ash within the North Atlantic (Lane et al., 2012; Table 1). The correlation of this tephra horizon to the Vedde Ash derives from the Late Glacial – Holocene age of the sediment sequence, the bimodal nature of the tephra identified in sample HBP2_21A and the geochemically indistinguishable composition to other VA horizons in the North Atlantic. In addition to total alkali silica plots, potassium and iron are commonly used in bi-plots to distinguish the Vedde Ash from other geochemically similar deposits from the Late Glacial – Holocene transition (Fig. 4; Lane et al., 2012; Haflidason et al., 2019; Høgaas et al., 2021; Supplementary).

3.3. Heftye-moraine and sediment chronology

Eight distinct samples (including shell fragments, mixed benthic foraminifera and terrestrial/aquatic macrofossils) were radiocarbon dated in order to constrain the age of the Heftyebreen moraine and lake sediment sequence. The landform and strata are further constrained in time by the presence of a cryptotephra horizon identified near the bottom of Unit 2 (Figs. 3, 4). All radiocarbon ages bracket the Late Glacial to Early Holocene (Fig. 3; Table S1). However, radiocarbon age reversals suggest some of the dated material may present anomalously old ages (Fig. 3). Due to low concentrations of terrestrial macros, aquatic bryophytes were also analyzed in samples at 239 and 234 cm (composite depth) in order to date the lower sediments in Unit 2. Ages 13.9 and 12.7 cal ka BP respectively, from the lacustrine sequence, are older than the shell fragments form the diamict as well as the Vedde Ash. Due to the identification of a cryptotephra isochron within this record, we are able to identify likely anomalously old radiocarbon ages. Given the geomorphological context of the Heftyevatnet basin, situated within the end moraine, we assume the moraine was formed and abandoned prior to sediment accumulation within the lake basin.

Two shell fragments of *Hiatella arctica,* collected from diamict within the 52 m terrace, suggest ice-free marine conditions between *c.* 12.9–12.8 cal ka BP (Fig. 2A; Table S1; Fig. S2). Shell ages indicate that inner Grønfjorden had deglaciated approximately 1.5 ka earlier than previously reconstructed (Mangerud et al., 1992). Furthermore, the ages provide a maximum constraining age on the deposition of the sediments in the 52 m terrace and the corresponding sharp-crested ridge. It is thus assumed that a local glacier re-advanced into a high relative sea level, and re-deposited the shell fragments while forming the curvilinear ridge (with an ice margin both in marine and subaerial environments). Only following the retreat of the local glacier did sediment begin to accumulate in the Heftye-basin. Therefore, the ages from the mollusc fragments within the diamict, additionally provide a maximum-limiting age constrain for the basal sediments in Heftyevatnet. No direct evidence of a subglacial facies has been identified (i.e. low angle thrusts) within the diamict. However, we suggest given the setting and diamict composition, the sediments must at least have a glacial proximal origin. Furthermore, we cannot fully negate that the shell fragments post-date the moraine. However, given their occurrence within the diamict as opposed to literal position within beach gravels (overlaying the diamict), the post-deposition of these shells in a shore-face environment seems less likely. If however, the shells were deposited post moraine formation, they were likely re-sediment shortly following moraine abandonment given the foraminifera age (at the base of the lake sequence) closely aligns with the 2-sigma of the younger shell fragment.

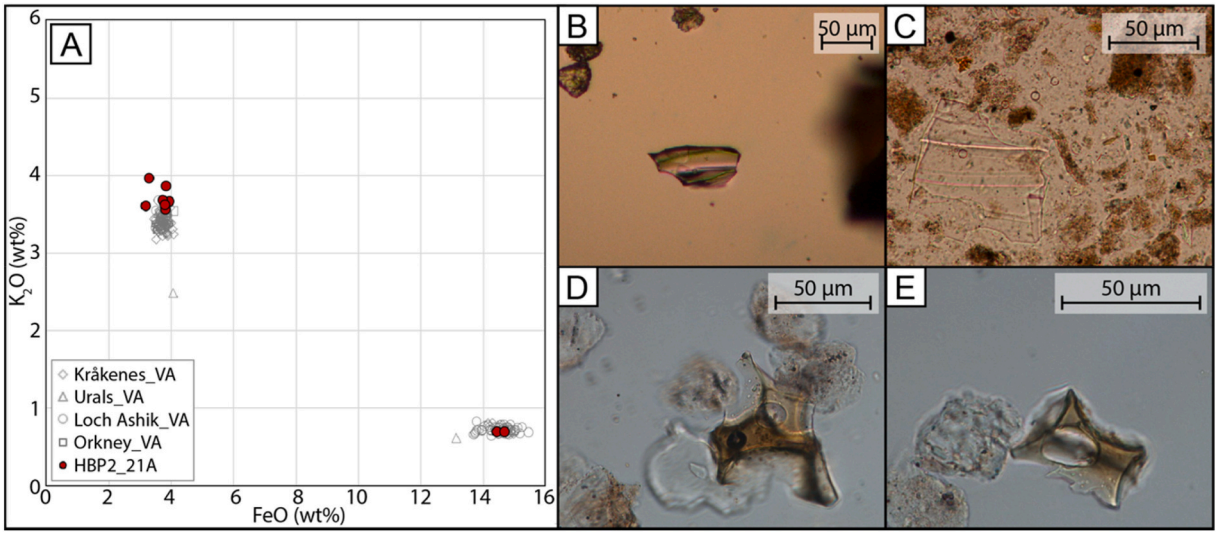

Fig. 4. Heftyevatnet cryptotephra bi-plot and photomosaic. A) Geochemical bi-plot comparing distally deposited Vedde Ash (VA) from Norway, Russia and Scotland to sample HBP2_21A from Heftyevatnet, Svalbard (Fig. S3; Lane et al., 2012; Timms et al., 2017; Haflidason et al., 2019). Microscopic imagery of sample HBP2_21A with examples of rhyolitic (B & C) and basaltic (D & E) tephra identified in the lowermost lacustrine sediments of Heftyevatnet. Micromanipulator controlled syringe visible (at right) in image B) photographed during tephra concentration. Images C-E were obtained from smear slides.

Table 1
Non-normalized mean major element values for the Vedde Ash tephra samples. The number of analyzed shards is shown in parentheses. Basaltic points were conducted on one large shard. SD refers to standard deviation. All analysis was conducted at the Institute of Earth Science, University of Iceland.

Sample		SiO_2	TiO_2	Al_2O_3	FeO	MnO	MgO	CaO	Na_2O	K_2O	P_2O_5	Total
HBP2_21A												
Vedde R	M	71,18	0,25	13,64	3,64	0,12	0,15	1,25	3,73	3,72	0,03	97,71
(7)	SD	1,08	0,05	0,48	0,29	0,03	0,10	0,11	1,14	0,15	0,02	2,42
Vedde B	M	46.84	4.68	12.69	14.56	0,23	5.10	9.76	2.68	0.70	0.56	97.78
(2[a])	SD	0.18	0.03	0.07	0.18	0.01	0.03	0.04	0.05	0.00	0.06	0.31

[a] Data reflects two probe readings taken from the same tephra shard.

Radiocarbon-dated benthic foraminifera (at 299 cm) and plant macrofossils (at 239, 234, 228 and 212 cm) constrain the timing of moraine formation and lake basin isolation from Grønfjorden. The most robust age constraint for the marine to lacustrine facies transition is the cryptotephra, occurring between 1 and 2 cm above this sedimentary boundary and limiting the basin isolation to roughly a century before 12.1 ka BP (12,225 yr. BP derived from the Bayesian statistics code BACON). Peak ash concentrations were identified within the lowermost interval of Unit 2, composed of finely laminated brown gyttja (sample HBP2_21A). Approximately 63 shards of rhyolitic and basaltic tephra per dried gram sediment were identified in the second cm of laminated organic rich lacustrine sediments overlaying the transition from marine basal sediments (Figs. 3, 4). Tephra shards were manually concentrated from the peak interval through micromanipulation prior to electron microprobe analysis detailing the major element composition of the glass (Fig. 4). Both rhyolitic and basaltic components of sample HBP2_21A (239-238 cm) indicate geochemical fingerprinting of the Katla volcanic system and the Vedde Ash (Figs. 4A and S3; Tables 1 and S3; Lane et al., 2012). The presence of the Vedde Ash at this interval in the Heftyevatnet sequence suggests that the lake basin isolated from the fjord before 12.1 ka BP (Andersen et al., 2006; Lane et al., 2013).

Given that the Heftyevatnet Vedde Ash was deposited in the lowermost lacustrine gyttja (Unit 2), stratigraphically above the marine sediments, the relative sea level must have already dropped below the lake threshold level of 43 m a.s.l. at the time of the eruption. Based on shell ages and the Vedde Ash, we assume the lower two radiocarbon dates (terrestrial/aquatic macrofossils at 239 and 234 cm composite depth) from Unit 2 exhibit anonymously old ages as they are older than the shells and Vedde Ash. With the given data, there is no means of discrediting the quality of the remaining radiocarbon ages (8.1 cal ka BP at 212 and 9.5 cal ka BP at 228 cm in Unit 2 and 12.5 cal ka BP at 299 cm depth in Unit 1), however further independent constraints (tephrochronology) may allow for testing the validity of these ages.

4. Discussion

4.1. Svalbard glaciers during the Younger Dryas period and the Heftyebreen moraine

Longstanding and robust evidence suggests that Spitsbergen's west-coast cirque glaciers were less extensive during the Late Glacial than the Late Holocene (Mangerud and Svendsen, 1990; Svendsen and Mangerud, 1997; Mangerud and Landvik, 2007). Until recently, the deglaciation of Svalbard has been considered as being continuous with uninterrupted retreat (Hormes et al., 2013). This is partly due to the apparent absence of moraines or other ice-marginal landforms dating to the YD chronozone (Forwick and Vorren, 2009; Hormes et al., 2013). The scarcity of ice-marginal features has been associated with deglaciation ice-shelves potentially influencing the nature of landform development and sedimentation (Farnsworth et al., 2018; Larsen et al., 2018; Noormets et al., 2021). Additionally, ice marginal retreat within fjord-systems has been proposed to have occurred during the YD in some areas (Larsen et al., 2018; Rasmussen and Thomsen, 2020). However, an increasing number of studies from around Svalbard have identified ice-marginal landforms deposited by glacier re-advances during the Late Glacial-Early Holocene (Salvigsen et al., 1990; Lønne, 2005; Henriksen et al., 2014; Farnsworth et al. 2017, 2018, 2020a; Flink et al., 2018; Larsen et al., 2018; Rasmussen and Thomsen, 2020).

We associate the diamict-composed, sharp-crested ridge and the accompanying 52 m terrace to the palaeo-Heftyebreen cirque glacier. We also suggest that the palaeo-glacier re-advanced into Grønfjorden's high (>52 m) relative sea level during the early YD chronozone, forming the frontal-lateral moraine at the mouth of the Heftyebreen catchment. Our interpretation is based on the curvilinear structure of the ridge and the 52 m terrace (with associated marine diamict) as well as the steeper northwestern (glacial proximal) flank. Presumably if the sea level has regressed below 52 m elevation prior to moraine formation, the morphology of the sharp crested ridge would have continued northward capping the terrace.

We interpret the sharp-crested ridge and the adjoining terrace as an end moraine, deposited by a tidewater cirque glacier in the Heftyevatnet catchment during the early YD chronozone. Previously, however, it has been suggested that the sharp-crested ridge may originate from the Aldegondabreen catchment (a cirque to the south of Heftyebreen), as a result of a surge event prior to 12 ka BP (Kokin and Mavlyudov, 2020). Their inferred age (based on cross-cutting relationship with sea level) is comparable to ours; however, we hypothesize the frontal-lateral moraine around the mouth of the Heftyebreen cirque indicates there must have been a glacier in the Heftye-catchment during ridge formation. The morphology of the ridge (prominent, sharp-crested, 16 m thick) is more characteristic of an end moraine than a medial moraine. Regardless of whether there was also a glacier on the southeastern margin of the moraine system, it was deposited prior to deposition of the basal sediments in Heftyevatnet. There are two lines of evidence support this interpretation: i) the basal sediments are laminated and undeformed and therefore bear no evidence of being overridden during a glacier re-advance and ii) radiocarbon ages from the basal sediments and from the diamict comprising the moraine are 12.5 and 12.8 ka BP respectively, suggesting basin sedimentation began immediately after moraine abandonment.

The Heftyebreen moraine is the first and (as of yet) only glacier margin constrained to the YD chronzone in Svalbard (Fig. 5A and B). Furthermore, the glacier seems to have retreated shortly after the formation of the moraine, within the early YD chronzone. According to our new chronological constraints, the Heftyebreen cirque glacier re-advanced into a high relative sea level, depositing the moraine after 12.8 ka BP and before 12.5 ka BP. The 12.1 ka BP Vedde Ash is a more reliable minimum-limiting age for the moraine, however, given the relative stratigraphic positions, we consider the 12.5 ka BP radiocarbon age a closer minimum-limiting constrain (Fig. 5A and B). While numerous other moraines have been effectively constrained to the Late Glacial – Early Holocene transition, none have been completely constrained to within the YD chronozone (Fig. 5; Mangerud et al., 1992; Lønne, 2005; Farnsworth et al., 2018; Larsen et al., 2018). Notably, where these Late Glacial – Early Holocene re-advances are identified, Late Holocene glacier expansion was minimal with some cirque and valley systems remaining nearly ice free during this period (Farnsworth et al., 2018), suggesting that more extensive Late Holocene glaciers may

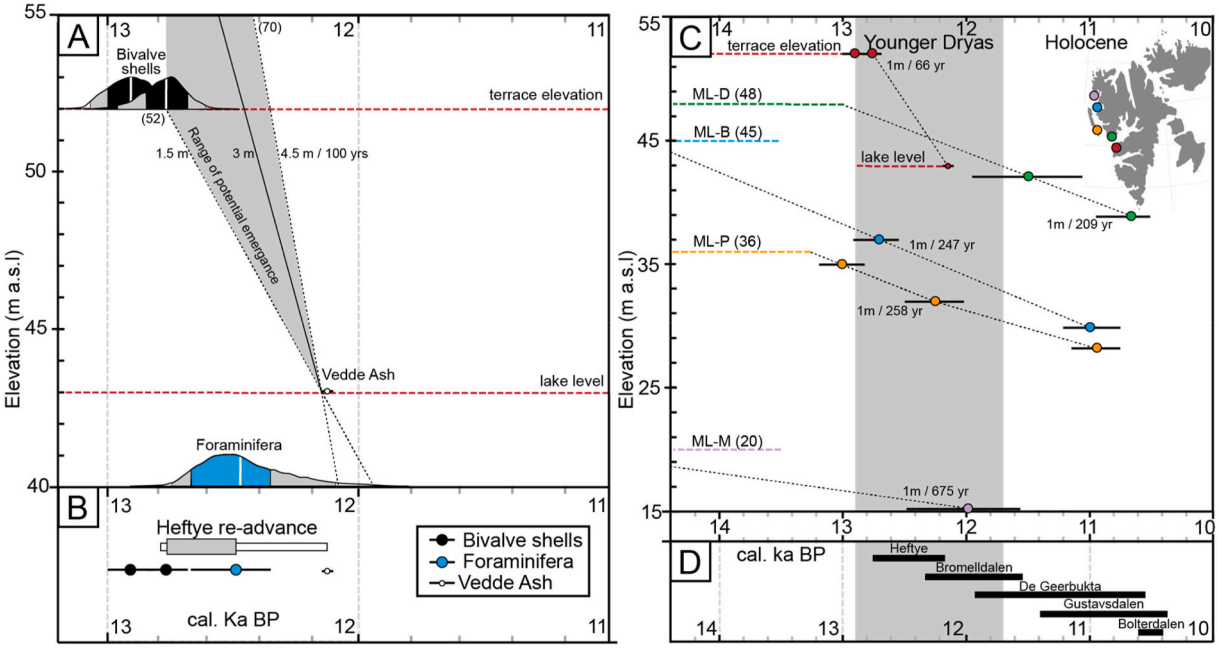

Fig. 5. Time – elevation plots exhibiting Late Glacial – Early Holocene emergence and glacier fluctuations. A) Plot indicating the range of potential emergence constrained by the shells within the 52-m terrace and the Vedde Ash within an isolation basin (threshold elevation 43 m a.s.l.). Shell fragments are interpreted to have been redeposited from the former glacier margin providing a maximum-limiting constraint for the age of the 52 m a.s.l. terrace and likely reflecting a relative sea level higher than the elevation at which they were deposited. Potential emergence rates range from 1.5 to 4.5 m per 100 years depending on the palaeo-sea level in which the shells reflect (>52 and <70 m). B) The Heftyebreen moraine is constrained between 12.8 and 12.5 cal ka BP by the shell fragments in the 52 m terrace and the basal age of mixed benthic foraminifera from the lowermost Heftyevatnet sediments. Furthermore, while the Vedde Ash best constrains the basin isolation, its presence in the lake record suggest Heftyebreen had advanced and retreated from the shallow marine environment prior to the eruption. C) Restrained rebound rates from Heftyebreen compared to other Late Glacial emergence curves from western Svalbard (Forman, 1990; Forman et al., 2004). All sea level curve ages have been re-corrected and calibrated (Table S2). D) The early Younger Dryas re-advance from Heftyebreen compared to other re-advances constrained to the Late Glacial - Early Holocene (Mangerud et al., 1992; Lønne, 2005; Farnsworth et al., 2018; Larsen et al., 2018). No clear synchronicity is exhibited in this series of glacier re-advances.

have removed older, potentially correlative deposits. Despite an increasing number of these dated ice margins with enhanced chronological constraint, there is no clear synchronicity among Late Glacial-Early Holocene glacier fluctuations. Thus, the ice-marginal behavior of some glacier systems during the Late Glacial-Early Holocene may have been controlled by internal glacier dynamics rather than by regional mass balance trends which would have presumably forced more synchronous ice-marginal oscillations.

4.2. Heftyevatnet and Late Glacial emergence

Shell fragments were eroded from marine sediments, transported and redeposited by a glacier into the diamict (capping the terrace) at an unknown palaeo-sea level, albeit greater than 52 m above present sea level. Although the shells may have been resedimented from higher or lower elevation, they provide a maximum-limiting age for the 52 m a.s.l. shoreline. Thus, the relative sea level dropped at least 9 m (from >52 m a.s.l. to below 43 m a.s.l.) in approximately 600 years (between 12.8 and 12.2 ka BP), yielding a minimum rate of emergence of 1.5 m per 100 years (1 m/66 yrs; Fig. 5A). If we assume the palaeo-sea was 70 m a.s.l. (like the marine limit at the mouth of Grønfjorden; Mangerud and Svendsen, 1990) during the re-sedimentation of the shells (by glacier re-advance), the rate would be 4.5 m per 100 years (Fig. 5A). The palaeo-sea level was likely between these two elevations and thus emergence rates may have been on the order of 3 m per 100 years. Despite variable ice thicknesses, ice-cover durations and deglaciation histories, relative sea level curves from western Svalbard generally suggest lower rates of Late Glacial emergence. Even the minimum emergence rate (1.5 m per 100 yrs) reconstructed from Heftyevatnet is roughly three times greater than that inferred from relative sea-level curves from western Svalbard (Fig. 5C; Forman, 1990; Forman et al., 2004). Two to 3 m of emergence over a 100 year period is similar to Early Holocene rates which have been reconstructed from raised shorelines (Forman et al., 2004; Farnsworth et al., 2020a). However, an emergence rate of two to 3 m per 100 years during the Late Glacial is significant as it may have impacted glacier dynamics during the deglaciation. Furthermore, such rates of emergence may indicate poorly understood restrained rebound prior to deglaciation.

Extensive efforts have been placed on radiocarbon dating postglacial raised shorelines around former ice sheet margins in order to constrain rates of postglacial uplift and subsequently provide input data for glacier models (Forman et al., 2004; Lecavalier et al., 2014; Simon et al., 2016). As a result, the rates and spatial variability of postglacial uplift are relatively well constrained in near-field regions. However, due to the lack of datable material and resolution, our understanding of the rates and magnitudes of restrained rebound (prior to shoreline formation) is limited (Andrews et al., 1970). Here we contribute directly to a quantitative reconstruction of restrained rebound in western Svalbard during the YD. Furthermore, our reconstructed minimum emergence rate highlights the under-represented crustal response to ice loss during this time.

While we know relatively little about glacier margins during the YD in Svalbard, we know even less about the regional equilibrium line altitude (ELA) at this time (Rea et al., 2020). Assuming that the ELA remained constant through the 1.2 ka YD period, with an emergence rate of 3 m per 100 years, we would expect roughly 33 m of vertical displacement (land passing up through the ELA). Although the process is non-linear (Andrews et al., 1970; Forman et al., 2004), as an approximation we can extend this estimate farther back in time to *c.* 14.6 ka BP, following the initiation of regional ice loss from the continental shelf

edge (Brendryen et al., 2020). This would suggest nearly 100 m of displacement (i.e. restrained rebound) may have occurred prior to the formation of beach ridges and measurable relative sea level.

Based on a reconstruction from western Svalbard, the ELA is suggested to have risen roughly ~50 m over the last 100 yrs, since the culmination of the Little Ice Age (Røthe et al., 2015). The regional ELA was certainly not constant during the transition from Late Glacial to Early Holocene. However, comparing emergence rates from this period with modern glacier response to rising ELA provides perspective regarding the potential effects of restrained rebound on Svalbard's sensitive glaciers (Noël et al., 2020). While modeling investigations incorporating restrained rebound in Iceland have indicated a significant effect on glacier dynamics and the regrowth of the Younger Dryas Ice Sheet, this has not yet been developed for other ice sheets (Norðdahl and Ingólfsson, 2015). A minimal glacier model that incorporates varying rates (and durations) of restrained rebound would be valuable to further enhance our understanding of these potential effects on glacier dynamics (Oerlemans, 2018).

4.3. Distally deposited tephra in Svalbard and future prospects

Despite occurring at low concentrations, the presence of distally-deposited tephra has a high potential to improve geochronology in the Arctic. While the VA cryptotephra is the first isochron from the Katla volcanic system to be identified in lake sediments from Svalbard, other tephra from Late Holocene eruptions of Hekla, Öræfajökull and Snæfellsjökull have previously been identified (D'Andrea et al., 2012). Furthermore, the identification of a Middle Holocene cryptotephra from Kamchatka highlights the potential of pan-Arctic cryptotephra deposition in Svalbard (van der Bilt et al., 2017). Outside of lacustrine archives, a historical tephra from Grímsvötn has been identified from ice cores from Svalbard (Kekonen et al., 2005; Wastegård and Davies, 2009). As well, ocean-rafted pumice from Katla has been collected from Holocene raised beaches (Blake, 1961; Farnsworth et al., 2020b). Tephra identified in Svalbard has enhanced our understanding of the distal deposition of the volcanic glass, the chronology of the substratum in which it was deposited, as well as in some cases the eruption history. It would be valuable for further work to develop a chronostratigraphic framework of tephra in Svalbard. Additionally, linking cryptotephra investigations to varved lake sediments may help better constrain the age of past eruptions (Lane et al., 2013). Furthermore, identification of tephra horizons from high resolution marine sedimentary archives would help test hypotheses regarding Late Glacial Holocene marine reservoir corrections around Svalbard.

5. Conclusions

Low concentrations of tephra have a high potential to improve geochronology in the Arctic. This study demonstrates that cryptotephra on Svalbard can provide reliable new age constraints for lacustrine sedimentary archives, glacial landforms and raised marine deposits. We successfully extend the tool of crypto-tephrochronology from beyond sedimentary sequences to landforms and processes.

- We describe the first cryptotephra horizon of Vedde Ash identified on Svalbard.
- For the first time, the cryptotephra isochron constrains glacial and sea level history – thus highlighting the great geochronological potential of non-visible tephra, especially when combined with other dating methods.
- The well-defined age of the Vedde Ash allows us to constrain a cirque glacier re-advance on Svalbard to the early Younger Dryas chronozone. This result indicates that Svalbard's glacier margins were more complex and dynamic during the Late Glacial than previously thought.
- Given cryptotephra deposition occurred prior to the regional deglaciation and subsequent to local beach ridge formation, this record provides an exclusive opportunity to reconstruct the rate of restrained rebound for the region.
- While large uncertainties remain with relative sea-level histories constrained by shell fragments, the combination of the well-defined age of the Vedde Ash allows us to highlight rates of Late Glacial (restrained) rebound were over three times greater than previous estimates from western Svalbard. We highlight the need to revise the Late Glacial portions of regional sea-level curves and emphasize new rates should be incorporated in future glacier and isostatic adjustment models.

Author contributions

W.R.F. conceived this work and wrote the paper with all co-authors contributing. Field mapping and sampling was conducted by W.R.F., O. I., M.R., A.S., S.B., L.A., H.J.H., and M.F. Drone data acquisition, digital elevation model processing and development was produced by E.S.M. Both K.H.K. and A.J.P. assisted with sediment core processing and chronology. Cryptotephra preparation, analysis and interpretation was done by W.R.F., M.K., and E.R.G. All authors contributed with interpretation and discussion of results.

Declaration of competing interest

The authors declare that they have no known competing financial interests or personal relationships that could have appeared to influence the work reported in this paper.

Acknowledgements.

Funding was provided by The Svalbard Environmental Protection Fund (Project 16/35), Svalbard Science Forum Arctic Field Grant, NRC and NordVULK (to WRF). We acknowledge S.M. Cohen and UNIS Logistics for transportation and field support. G.H. Guðfinnsson is kindly acknowledged for support with the electron microprobe. The authors acknowledge two anonymous reviewers for their detailed and constructive comments.

Appendix A. Supplementary data

Supplementary data to this article can be found online at https://doi.org/10.1016/j.qsa.2021.100041.

References

Andersen, K.K., Svensson, A., Johnsen, S.J., Rasmussen, S.O., Bigler, M., Röthlisberger, R., Ruth, U., Siggaard-Andersen, M.-L., Steffensen, J.P., Dahl-Jensen, D., Vinther, B.M., Clausen, H.B., 2006. The Greenland Ice Core Chronology 2005, 15-42 ka. Part 1: constructing the time scale. Quat. Sci. Rev. 25, 3246–3257.

Andrews, J.T., Buckley, J.T., England, J.H., 1970. Late-glacial chronology and glacio-isostatic recovery, home bay, east baffin island, Canada. Geol. Soc. Am. Bull. 81, 1123–1148.

Blake Jr., W., 1961. Radiocarbon dating of raised beaches in Nordaustlandet, Spitsbergen. In: Raasch, G.O. (Ed.), Geology of the Arctic. University of Toronto Press, Toronto, pp. 133–145.

Brader, M.D., Lloyd, J.M., Barlow, N.L.M., Norðdahl, H., Bentley, M.J., Newton, A.J., 2017. Postglacial relative sea-level changes in northwest Iceland: evidence from isolation basins, coastal lowlands and raised shorelines. Quat. Sci. Rev. 169, 114–130.

Benediktsson, I.Ö., Schomacker, A., Johnson, M.D., Geiger, A., Ingolfsson, O., Guðmundsdóttir, E.R., 2015. Architecture and structural evolution of an early Little Ice Age terminal moraine at the surge-type glacier Múlajökull, Iceland. Journal of Geophysical Research Earth Surface 120–9, 1895–1910.

Besl, P., McKay, N., 1992. A method for registration of 3-D shapes. Proc. SPIE 1611, sensor fusion IV: control paradigms and data structures. Trans. PAMI 14. https://doi.org/10.1117/12.57955.

Blaauw, M., Christen, J.A., 2011. Flexible paleoclimate age-depth models using an auto regressive gamma process. Bayesian Analysis 6, 457–474.

Brendryen, J., Haflidason, H., Yokoyama, Y., Haaga, K.A., Hannisdal, B., 2020. Eurasian ice sheet collapse was a major source of Meltwater Pulse 1A 14,600 years ago. Nat. Geosci. https://doi.org/10.1038/s41561-020-0567-4.

Croudace, I.W., Rindby, A., Guy Rothwell, R., 2006. ITRAX: description and evaluation of a new multi-function X-ray core scanner. Geological Society, London, Special Publications 267, 51. https://doi.org/10.1144/gsl.sp.2006.267.01.04.
Carrivick, J.L., Smith, M.W., Quincey, D.J., 2016. Structure from Motion in the Geosciences. Wiley-Blackwell, Oxford, UK, p. 208.
D'Andrea, W.J., Vaillencourt, D.A., Balascio, N.L., Werner, A., Roof, S.R., Retelle, M., Bradley, R.S., 2012. Mild Little Ice Age and unprecedented recent warmth in an 1800-year lake sediment record from Svalbard. Geology 40, 1007–1010.
Dallmann, W.K., 2015. Geoscience atlas of svalbard. Norsk Polarinstitutt Rapportserie 148, 1–292.
Davies, S., Abbott, P.M., Pearce, N.J., Wastegård, S., Blockley, S.P.E., 2012. Integrating the INTIMATE records using tephrochronology: rising to the challenge. Quat. Sci. Rev. 36, 11–27.
Davies, S.M., 2015. Cryptotephras: the revolution in correlation and precision dating. J. Quat. Sci. 30, 114–130.
Dugmore, A.J., Larsen, G., Newton, A.J., 1995. Seven tephra isochrones in Scotland. Holocene 5, 257–266.
Farnsworth, W.R., Ingolfsson, O., Noormets, R., Allaart, L., Alexanderson, H., Henriksen, M., Schomacker, A., 2017. Dynamic Holocene glacial history of st. Jonsfjorden, svalbard. Boreas 46, 585–603.
Farnsworth, W.R., Ingolfsson, O., Retelle, M., Allaart, L., Håkansson, L., Schomacker, A., 2018. Svalbard glaciers re-advanced during the Pleistocene-Holocene transition. Boreas 47, 1022–1032.
Farnsworth, W.R., Allaart, L., Ingolfsson, O., Alexanderson, H., Forwick, M., Noormets, R., Retelle, M., Schomacker, A., 2020a. Holocene glacial history of Svalbard - status, perspectives and challenges. Earth Sci. Rev. 208, 103249.
Farnsworth, W.R., Blake Jr., W., Guomundsdottir, E.R., Ingolfsson, O., Kalliokoski, M.H., Larsen, G., Newton, A.J., Óladóttir, B.A., Schomacker, A., 2020b. Ocean-rafted pumice constrains postglacial relative sea-level and supports Holocene ice cap survival. Quat. Sci. Rev. 250, 106654.
Flink, A.E., Hill, P., Noormets, R., Kirchner, N., 2018. Holocene glacial evolution of Mohnbukta, in eastern Spitsbergen. Boreas 47, 390–409.
Forman, S.L., 1990. Post-glacial relative sea-level history of northwestern Spitsbergen, Svalbard. Geol. Soc. Am. Bull. 102, 1580–1590.
Forman, S.L., Lubinski, D.J., Ingolfsson, O., Zeeberg, J.J., Snyder, J.A., Siegert, M.J., Matishov, G.G., 2004. A review of postglacial emergence on svalbard, franz josef land and novaya zemlya, northern eurasia. Quat. Sci. Rev. 23, 1391–1434.
Forwick, M., Vorren, T.O., 2009. Late weichselian and Holocene sedimentary environments and ice rafting in isfjorden, spitsbergen. Palaeogeogr. Palaeoclimatol. Palaeoecol. 280, 258–274.
Haflidason, H., Regnéll, C., Pyne-O'Donnell, S., Svendsen, J.I., 2019. Extending the known distribution of the Vedde ash into siberia: occurrence in lake sediments from the timan ridge and the ural mountains, northern Russia. Boreas 48, 444–451.
Heaton, T.J., Köhler, P., Butzin, M., Bard, E., Reimer, R.W., Austin, W.E.N., Bronk, C.B., Grootes, P.M., Hughen, K.A., Kromer, B., Reimer, P.J., Adkins, J., Burke, A., Cook, M. S., Olsen, J., Skinner, L., 2020. Marine20-the marine radiocarbon age calibration curve (0-55,000 cal BP). Radiocarbon 62, 1–43.
Henriksen, M., Alexanderson, H., Landvik, J.Y., Linge, H., Peterson, G., 2014. Dynamics and retreat of the late weichselian kongsfjorden ice stream, NW svalbard. Quat. Sci. Rev. 92, 235–245.
Hormes, A., Gjermundsen, E.F., Rasmussen, T.L., 2013. From mountain top to the deep sea—deglaciation in 4D of the northwestern Barents Sea ice sheet. Quat. Sci. Rev. 75, 78–99.
Hughes, A.L.C., Gyllencreutz, R., Lohne, Ø.S., Mangerud, J., Svendsen, J.I., 2016. The last Eurasian ice sheets—a chronological database and time-slice reconstruction, DATED-1. Boreas 45, 1–45.
Høgaas, F., Larsson, S.A., Klug, M., Olsen, L., Wastegård, S., 2021. Palaeolake sediment records reveal a mid- to late Younger Dryas ice-sheet maximum in Mid-Norway. Boreas. https://doi.org/10.1111/bor.12543. ISSN 0300-9483.
Jakobsson, M., et al., 2012. The international bathymetric chart of the arctic ocean (IBCAO) version 3.0: IBCAO version 3.0. Geophys. Res. Lett. 39, L12609. https://doi.org/10.1029/2012GL052219.
James, M.R., Robson, S., Smith, M.W., 2017. 3-D uncertainty-based topographic change detection with structure-from-motion photogrammetry: precision maps for ground control and directly georeferenced surveys: 3-D uncertainty-based change detection for SfM surveys. Earth Surf. Process. Landforms 12, 1769–1788. https://doi.org/10.1002/esp.4125.
Kalliokoski, M., Guðmundsdottir, E.R., Wastegård, S., 2020. Hekla 1947, 1845, 1510 and 1158 tephra in Finland: challenges of tracing tephra from moderate eruptions. J. Quat. Sci. 35, 803–816. https://doi.org/10.1002/jqs.3228.
Kekonen, T., Moore, J., Perämäki, P., Mulvaney, R., Isaksson, E., Pohjola, V., van de Wal, R.S.W., 2005. The 800-year long ion record from the Lomonosovfonna (Svalbard) ice core. J. Geophys. Res. 110, D07304.
Kokin, O., Mavlyudov, B., 2020. Geological and geomorphological indicators of the surge behavior of the aldegonda glacier (west spitsbergen) in the little ice age (in Russian). Geomorfologiya 81–95. https://doi.org/10.31857/S0435428120010071.
Kylander, M.E., Ampel, L., Wohlfarth, B., Veres, D., 2011. High-resolution XRF core scanning analysis of Les Echets (France) Sedimentary sequence: new insights from chemical proxies. J. Quat. Sci. 26, 109–117.
Larsen, N.K., Strunk, A., Levy, L.B., Olsen, J., Bjørk, A., Lauridsen, T.L., Jeppesen, E., Davidson, T.A., 2017. Strong altitudinal control on the response of local glaciers to Holocene climate change in southwest Greenland. Quat. Sci. Rev. 168, 69–78.
Larsen, E.A., Lyså, A., Rubensdotter, L., Farnsworth, W.R., Jensen, M., Nadeau, M.J., Ottesen, D., 2018. Late-glacial and Holocene glacier activity in the van mijenfjorden area, western svalbard. Arktos 4, 9. https://doi.org/10.1007/s41063-018-0042-2.
Lane, C.S., Blockley, S.P.E., Mangerud, J., Smith, V.C., Lohne, Ø.S., Tomlinson, E.L., Matthews, I.P., Lotter, A.F., 2012. Was the 12.1 ka Icelandic Vedde Ash one of a kind? Quat. Sci. Rev. 33, 87–99.
Lane, C.S., Brauer, A., Blockley, S.P.E., Dulski, P., 2013. Volcanic ash reveals time-transgressive abrupt climate change during the Younger Dryas. Geology 41, 1251–1254.
Lecavalier, B.S., Milne, G.A., Simpson, M.J.R., Wake, L., Huybrechts, P., Tarasov, L., Kjeldsen, K.K., Funder, S., Long, A.J., Woodroffe, S., Dyke, A.S., Larsen, N.K., 2014. A model of Greenland ice sheet deglaciation constrained by observations of relative sea level and ice extent. Quat. Sci. Rev. 102, 54–84.
Lowe, D.J., 2011. Tephrochronology and its application: a review. Quat. Geochronol. 6, 423.
Lønne, I., 2005. Faint traces of high Arctic glaciations: an early Holocene ice-front fluctuation in Bolterdalen, Svalbard. Boreas 34, 308–323.
Mangerud, J., Lie, S.E., Furnes, H., Kristiansen, I.L., Lømo, L., 1984. A Younger Dryas ash bed in western Norway, and it's possible correlations with tephra in cores from the Norwegian Sea and the North Atlantic. Quaternary Research 21, 85–104.
Mangerud, J., Svendsen, J.I., 1990. Deglaciation chronology inferred from marine sediments in a proglacial lake basin, western Spitsbergen, Svalbard. Boreas 19, 249–272.
Mangerud, J., Bolstad, M., Elgersma, A., Helliksen, D., Landvik, J.Y., Lønne, I., Lycke, A. K., Salvigsen, O., Sandahl, T., Svendsen, J.I., 1992. The last glacial maximum on Spitsbergen, Svalbard. Quaternary Research 38, 1–31.
Mangerud, J., Bondevik, S., Gulliksen, S., Hufthammer, A., Høisæter, T., 2006. Marine 14C reservoir ages for 19th century whales and molluscs from the North Atlantic. Quat. Sci. Rev. 25, 3228–3245.
Mangerud, J., Landvik, J.Y., 2007. Younger Dryas cirque glaciers in western spitsbergen: smaller than during the little ice age. Boreas 36, 278–285.
Muschitiello, F., Pausata, F.S.R., Lea, J.M., Mair, D.W.F., Wohlfarth, B., 2017. Enhanced ice sheet melting driven by volcanic eruptions during the last deglaciation. Nat. Commun. 8, 1020. https://doi.org/10.1038/s41467-017-01273-1.
Noël, B., Jakobs, C.L., van Pelt, W.J.J., Lhermitte, S., Wouters, B., Kohler, J., Hagen, J.O., Luks, B., Reijmer, C.H., van der Verg, W.J., van den Broeke, M.R., 2020. Low elevation of Svalbard glaciers drives high mass loss variability. Nat. Commun. 11, 4597. https://doi.org/10.1038/s41467-020-18356-1.
Norodahl, H., Ingolfsson, O., 2015. Collapse of the Icelandic ice sheet controlled by sea level rise? Arktos 1, 13. https://doi.org/10.1007/s41063-015-0220-x.
Norðdahl, H., Haflidason, H., 1992. The skógar tephra, a younger Dryas marker in north Iceland. Boreas 21, 23–41.
Noormets, R., Flink, A., Kirchner, N., 2021. Glacial dynamics and deglaciation history of Hambergbukta reconstructed from submarine landforms and sediment cores, SE Spitsbergen, Svalbard. Boreas 50, 29–50. https://doi.org/10.1111/bor.12488.
Oerlemans, J., 2018. Modelling the late Holocene and future evolution of Monacobreen, northern Spitsbergen. Cryosphere 12, 3001–3015. https://doi.org/10.5194/tc-12-3001-2018.
Pilcher, J.R., Hall, V.A., 1992. Towards a tephrochronology for the Holocene of the north of Ireland. Holocene 2, 255–259.
Rasmussen, T.L., Thomsen, E., 2020. Climate and ocean forcing of ice-sheet dynamics along the Svalbard-Barents Sea Ice Sheet during the deglaciation ~20,000–10,000 years BP. Quaternary Science Advances. https://doi.org/10.1016/j.qsa.2020.100019.
Rea, B.R., Pellitero, R., Spagnolo, M., Hughes, P., Ivy-Ochs, S., Renssen, H., Ribolini, A., Bakke, J., Lukas, S., Braithwaite, R.J., 2020. Atmospheric circulation over europe during the younger Dryas. Science Advances 6, eaba4844.
Reimer, P.J., Austin, W.E.N., Bard, E., Bayliss, A., Blackwell, P.G., Ramsey, C.B., Butzin, M., Cheng, H., Edwards, R.L., Friedrich, M., Grootes, P.M., Guilderson, T.P., Hajdas, I., Heaton, T.J., Hogg, A.G., Hughen, K., Kromer, B., Manning, S.W., Muscheler, R.J., Palmer, G., Pearson, C., van der Plicht, J., Reimer, R.W., Richards, D.A., Scott, E.M., Southon, J.R., Turney, C.S.M., Wacker, L., Adolphi, F., Büntgen, U., Capano, M., Fahrni, S., Fogtmann-Schulz, A., Friedrich, R., Miyake, F., Olsen, J., Reinig, F., Sakamoto, M., Sookdeo, A., Talamo, S., 2020. The IntCal20 northern hemisphere radiocarbon age calibration curve (0-55 cal kBP). Radiocarbon 62, 725–757.
Rundgren, M., Ingolfsson, O., Björck, S., Jiang, H., Haflidason, H., 1997. Dynamic sea level change during the last deglaciation of northern Iceland. Boreas 26, 200–215.
Røthe, T.O., Bakke, J., Vasskog, K., Gjerde, M., D'Andrea, W.J., Bradley, R.S., 2015. Arctic Holocene glacier fluctuations reconstructed from lake sediments at Mitrahalvøya, Spitsbergen. Quat. Sci. Rev. 109, 111–125.
R Core Team, 2020. R: A Language and Environment for Statistical Computing. R Foundation for Statistical Computing, Vienna, Austria. Retrieved from. https://www.R-project.org/.
Salvigsen, O., Elgersma, A., Hjort, C., Lagerlund, E., Liestøl, O., Svensson, N.-O., 1990. Glacial history and shoreline displacement on erdmannflya and bohemanflya, spitsbergen, svalbard. Polar Res. 8, 261–273.
Schomacker, A., Krüger, J., Larsen, G., 2003. An extensive late Holocene glacier advance of Kötlujökull, central south Iceland. Quat. Sci. Rev. 22, 1427–1434.
Schomacker, A., Farnsworth, W.R., Ingolfsson, O., Allaart, L., Håkansson, L., Retelle, M., Siggaard-Andersen, M.-L., Korsgaard, N.J., Rouillard, A., Kjellman, S.E., 2019. Postglacial relative sea level change and glacier activity in the early and late Holocene: wahlenbergfjorden, Nordaustlandet, Svalbard. Sci. Rep. 9 (1–13), 6799.
Simon, K.M., James, T.S., Henton, J.A., Dyke, A.S., 2016. A glacial isostatic adjustment model for the central and northern Laurentide Ice Sheet based on relative sea level and GPS measurements. Geophys. J. Int. 205, 1618–1636.
Svendsen, J.I., Mangerud, J., 1997. Holocene glacial and climatic variations on Spitsbergen, Svalbard. Holocene 7, 45–57.

Timms, R.G.O., Matthews, I.P., Palmer, A.P., Candy, I., Abel, L., 2017. A high-resolution tephrostratigraphy from quoyloo meadow, orkney, Scotland: implications for the tephrostratigraphy of NW europe during the last glacial-interglacial transition. Quat. Geochronol. 40, 67–81.

Turney, C.S.M., 1998. Extraction of the rhyolitic component of Vedde microtephra from minerogenic lake sediments. J. Paleolimnol. 19, 199–206.

van der Bilt, W.G.M., Lane, C.S., 2019. Lake sediments with Azorean tephra reveal ice-free conditions on coastal northwest Spitsbergen during the Last Glacial Maximum. Sci. Adv. 5 (eaaw5980.).

van der Bilt, W.G.M., Lane, C.S., Bakke, J., 2017. Ultra-distal Kamchatkan ash on Arctic Svalbard: towards hemispheric cryptotephra correlation. Quat. Sci. Rev. 164, 230–235.

Wastegård, S., Davies, S., 2009. An overview of distal tephrochronology in northern Europe during the last 1000 years. J. Quat. Sci. 24, 500–512.

Wastegård, S., Guðmundsdottir, E.R., Lind, E.M., Timms, R.G.O., Björck, S., Hannon, G. E., Olsen, J., Rundgren, M., 2018. Towards a Holocene tephrochronology for the Faroe Islands, north Atlantic. Quat. Sci. Rev. 195, 195–214.

Wolfe, A.P., Miller, G.H., Olsen, C.A., Forman, S.L., Doran, P.T., Holmgren, S.U., 2004. Geochronology of high latitude lake sediments. In: Long-Term Environmental Change in Arctic and Antarctic Lakes, Developments in Paleoenvironmental Research. Springer, Dordrecht, pp. 19–52. https://doi.org/10.1007/978-1-4020-2126-8_2.

xdem contributors, 2021. Xdem. Zenodo. https://doi.org/10.5281/ZENODO.4809697.

Zamelczyk, K., Rasmussen, T.L., Husum, K., Haflidason, H., de Vernal, A., Ravna, E.K., Hald, M., Hillaire-Marcel, C., 2012. Paleoceanographic changes and calcium carbonate dissolution in the central Fram Strait during the last 20 ka yr. Quaternary Research 78, 405–416.